Available online at www.sciencedirect.com
ScienceDirect
Journal of Magnetic Resonance 182 (2006) 126–132
JMR Journal of Magnetic Resonance
www.elsevier.com/locate/jmr

Design of an inductively decoupled microstrip array at 9.4 T

Bing Wu [a], Xiaoliang Zhang [b], Peng Qu [a], Gary X. Shen [a,*]

[a] MRI Lab, Department of Electrical and Electronics Engineering, The University of Hong Kong, Hong Kong
[b] Center for Magnetic Resonance Research, Medical School, University of Minnesota, Minneapolis, MN, USA

Received 5 January 2006; revised 30 March 2006
Available online 7 July 2006

Abstract

By independent control of the phases and amplitudes of its elements, the microstrip transmission-line array can mitigate sample-induced RF non-uniformities, and has been widely used as the transceiver in parallel imaging applications. One major challenge in implementing the microstrip array is the reduction of mutual coupling among individual elements. The low-input impedance preamplifier is commonly used for the decoupling purpose. However, it is impractical in the transceiver array design. Although interconnecting capacitors can be utilized to reduce the mutual coupling, they only efficiently work for the neighbor elements. In addition, this approach is impractical at fields higher than 300 MHz, in which the required decoupling capacitance is commonly less than 0.5 pF. We propose a novel decoupling approach by using decoupling inductors in this study. Due to the fact that the decoupling inductance is independent of the resonant frequency, the microstrip arrays can be well decoupled at ultra-high fields. To verify the proposed approach, an eight-channel microstrip array is fabricated and tested at 9.4 T. For this prototype, couplings between elements are significantly reduced by using the interconnecting inductors. The phantom experiment shows that the inductively decoupled microstrip array has good parallel imaging performance.

Keywords: RF coil; Decoupling circuit; Microstrip transmission-line array; Ultra-high field

1. Introduction

The major advantages provided by high magnetic fields are increased NMR sensitivity, ultimately improved spatial and spectral resolution. For parallel imaging strategies based on multi-coil arrays [1,2], high fields are expected to improve parallel imaging performance due to the more complex sensitivity profiles of each coil element and the increased signal-to-noise ratio (SNR) [3,4]. However, there are some significant challenges in the image acquisition at ultra-high fields. For example, the lack of body resonators for homogeneous transmit pulses and the non-uniform B_1 profile with human load. For the receive-only coil array, the limited space of the high field magnet sometimes makes it hard to use an additional volume coil for transmit. The volume microstrip transmission-line array [5–9] is one possible approach to overcome these limitations. With independent phase and amplitude control of its elements, it can mitigate the sample-induced RF non-uniformities and can be used for transmission and reception. The radiation loss is well addressed by coil designs that incorporate a ground plane into the resonance structure in the form of transmission-line. Without the need of a transmit coil, the array structure is more compact and hence valuable space is saved inside the ultra-high-field magnets.

One major challenge in implementing the microstrip transmission-line arrays is to find sufficient means to minimize mutual coupling between individual coil elements. In some cases, coil elements are intrinsically decoupled without resorting to additional decoupling circuits, e.g., when there are enough spacing between the resonant elements, or the thin substrate is selected to provide enough broad decoupling [5,8]. However, if the substrate thickness is increased to pursue deeper B_1 field penetration, or the coil array is built with narrow gap between coil elements, the mutual coupling among coils may be strong enough

* Corresponding author. Fax: +852 2559 8738.
E-mail address: gxshen@eee.hku.hk (G.X. Shen).

1090-7807/$ - see front matter
doi:10.1016/j.jmr.2006.04.013

to cause the resonance peak to split. Hence, the additional decoupling circuit is necessary to isolate individual coil elements. This becomes particularly important in transceiver arrays where low-input impedance preamplifier decoupling [10] is not easily feasible. Alternative methods for decoupling such as decoupling network [11] or compensating for the nearest neighbor mutual coupling by introduction of a capacitor [5–7,12,13] are currently used for microstrip arrays. However, extending the decoupling network to large numbers of elements (>8) is quite complex and challenging. The method by using interconnecting capacitors also has a problem for the fields higher than 7 T, where the required decoupling capacitance is usually unpractically small.

In this study, a novel inductive decoupling approach is presented. Unlike the transformer decoupling method [14] by using two coupled inductors, our approach is to interconnect inductors between adjacent microstrip elements for decoupling. This decoupling inductance is independent of the resonant frequency and therefore the microstrip array can be extended for the fields higher than 7 T. An eight-channel prototype at 9.4 T has been fabricated and tested to validate the proposed method.

2. Method and materials

2.1. Theory

Consider a pair of microstrip resonantors that are tuned to the same resonant frequency. The corresponding equivalent LC circuit is shown in Fig. 1a, where L and M are the self-inductance and mutual inductance, respectively. Let V_1 and V_2 denote the voltages of T_1–T_1' and T_2–T_2', and I_1, I_2 represent the currents in the two resonators, respectively.

If the two resonators are planar structures, or closely placed around a cylinder such that the induced current on the strip has the opposite direction to its original current, the coupling equations of the two-port network from T_1–T_1' to T_2–T_2' are

$$V_1 = j\omega L I_1 - j\omega M I_2$$
$$V_2 = j\omega L I_2 - j\omega M I_1. \qquad (1)$$

The second terms on the right-hand-side of Eq. (1) are the induced voltages. Note that V_1 and V_2 are reduced due to the mutual inductance has a negative sign. Based on Eq. (1), the $\boldsymbol{Z}$ parameters can be obtained as follows:

$$\boldsymbol{Z} = \begin{bmatrix} j\omega L & -j\omega M \\ -j\omega M & j\omega L \end{bmatrix}. \qquad (2)$$

According to this $\boldsymbol{Z}$ matrix, the two-port network from T_1–T_1' to T_2–T_2' can be replaced by a T-type circuit, which is shown in Fig. 1b.

Fig. 1c depicts two coupled microstrip resonators with an interconnecting inductor for decoupling. Two shunt capacitors C_1' and C_2' are placed at the ends of the striplines, and a serial capacitor C_2'' is placed on the strip for

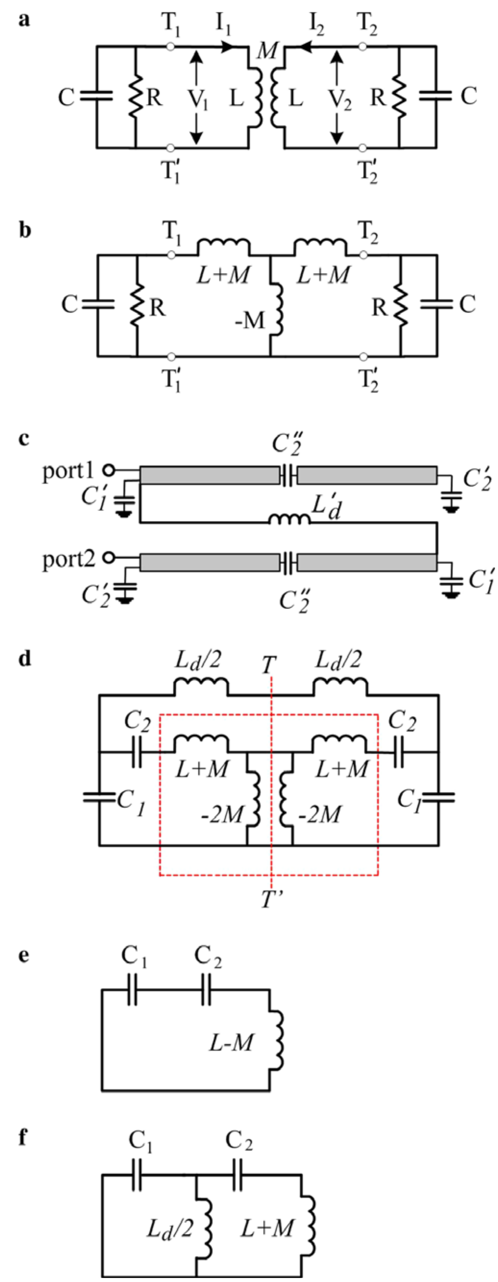

Fig. 1. The circuit of two coupled microstrip resonators (a) and its equivalent circuit (b). (c) Schematic of the coupled microstrip coils with a decoupling inductor. (d) Equivalent circuit of the coupled microstrip coils with decoupling inductor. (e) The circuit to calculate magnetic wall frequency by inserting an open circuit into T–T' of (d). (f) The circuit to calculate electric wall frequency by inserting a short circuit into T–T' of (d).

frequency tuning. Here L_d' is the decoupling inductance, C_1' locates between the ground and the connection point of the decoupling inductor L_d'.

The equivalent circuit of inductively decoupled microstrip resonators is shown in Fig. 1d. T-type coupling circuit is marked in a dashed square box. Note that the long connection trace of the decoupling inductor may have the reactance in series with the decoupling inductor. If this trace is placed closely to the ground plane, parasitic capacitor also exists between the trace and ground planes adjacent to it. Those reactance need to be considered in the equivalent circuit. Hence L_d in Fig. 1d is defined as the total reactance of the decoupling inductance L'_d and its connecting traces. C_1, which locates between L_d and the ground plane, is the total capacitance of C'_1 and the parasitic capacitance. C_2 is the equivalent capacitance of C'_2, C''_2 and the distributed shunt capacitance of the transmission-line, which is serial with C_1 in the microstrip coil. For simplicity, the resistance R in the equivalent LC loops is ignored and the decoupling inductor L_d is divided into two serial inductors with value of $L_d/2$ such that the circuit is symmetry from the line T–T'.

Based on the symmetry circuit in Fig. 1d, the two resonate frequencies of the coupled microstrip resonators, f_e and f_m, are calculated and the decoupling condition is obtained. According to "magnetic/electric wall" analysis [15], the symmetry circuit can be analyzed by inserting an open circuit (magnetic wall) and a short circuit (electric wall) into T–T'. Any bisection magnetic and electric circuit, which are shown in Figs. 1e and f, respectively, is used to calculate the resonant frequencies.

From the circuits in Figs. 1e and f, we have

$$\omega_m^2 = \frac{C_1 + C_2}{C_1 C_2 (L - M)} \tag{3}$$

$$\omega_e^2 C_2 \left(\frac{L_d/2}{2 - \omega_e^2 L_d C_1/2} + L + M \right) = 1 \tag{4}$$

where $\omega_{e,m} = 2\pi f_{e,m}$. When the two microstrip coils are totally decoupled, that is $\omega_e = \omega_m$, from Eqs. (3) and (4), the required L_d is expressed as follows,

$$L_d = L \cdot \frac{k^2(1 - m^2) + 2km(1 - m)}{m(1 + k)^2}, \tag{5}$$

where $k = C_2/C_1$ and $m = M/L$. Note that in Eq. (5), the required inductor L_d is determined by m, k, and L, and is independent of the resonant frequency. Hence the inductive decoupling method can be applied for microstrip arrays at ultra-high fields. Based on Eq. (5), the relations among L_d, m and k are further illustrated in Fig. 2 by assuming $L = 0.5$ μH. As shown in the figure, when $m < 0.2$ (this condition is usually satisfied for microstrip arrays at ultra-high fields), the required decoupling inductances can be adjusted in a board range by varying k.

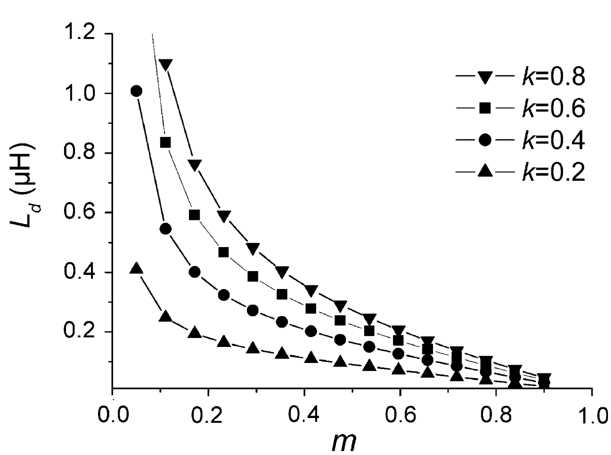

Fig. 2. The relationship between m and decoupling inductance L_d (assuming the self inductance $L = 0.5$ μH).

2.2. Coil construction

An eight-channel microstrip volume array was fabricated for mice imaging at 9.4 T (Fig. 3). The dimension of the cylinder former was 9.0 cm in length, 7.6 cm in outer diameter and 6.4 cm in inner diameter. The substrate used for the coil array was PETT, with a low loss tangent δ of 0.00015 and a permittivity of 2.1. The 6 mm substrate thickness for this prototype was selected according to the suggestion in Ref. [16]. The eight microstrip coils were built with 6.5 mm wide top strips and 2.5 cm wide ground strips. The inter-spacing between the strips was 2.0 cm and the inter spacing between the ground strips was 0.5 cm. Each element was matched to 50 Ω with a tunable capacitor (Voltronics, Denville, NJ) when loaded. The decoupling inductor was mounted via the gap between the ground strips such that the space inside the volume can be saved.

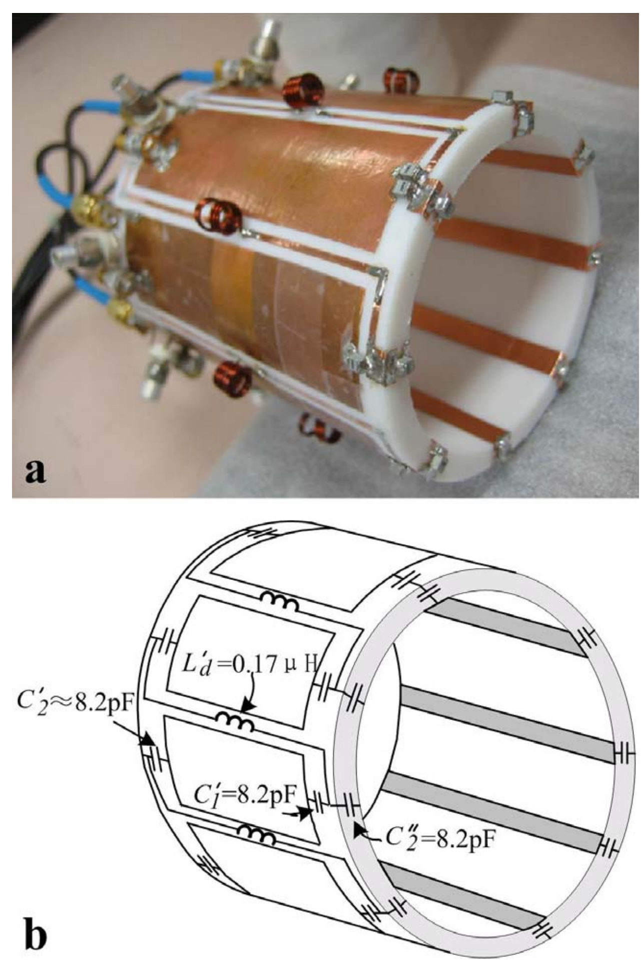

Fig. 3. Photograph (a) and sketch (b) of the eight-channel strip array for 9.4 T.

Two shunt capacitors C'_1, C'_2 and a serial capacitor C''_2 with the values around 8.2 pF were mounted on each element.

Bench experiments by observing the phase response from the S parameters [15] can prove that the mutual inductance between adjacent elements of the prototype is negative and, thus, the established inductive decoupling model is applicable. Each decoupling inductance is 0.18 μH (measured by a LCR meter, Agilent 4263B, at 100 KHz) which was wound with a copper wire of 7 turns and 7.0 mm in diameter. Note that the decoupling inductor here is somewhat a solenoidal coil. However, in this approach, k was tuned to decrease the decoupling inductance, such that its self-resonance frequency was well beyond the frequency of interest. In this prototype, the self-resonant frequencies of the decoupling inductors were around 800 MHz.

2.3. Experiment

To illustrate the advantages of this inductive decoupling method, it was compared to the conventional capacitive decoupling method [5] on bench. By varying the tuning capacitors on the strips, two adjacent microstrip elements in the prototype were tuned to the frequencies ranging from 200 MHz to 450 MHz, while the other six elements were open-circuit. This frequency range is commonly used for most high field applications. For each investigated frequency, all tuning capacitors C'_1, C'_2, and C''_2 were approximately equal, such that k in Eq. (5) approximates a constant.

Bench measurements were also taken to show the decoupling performance with different phantoms. Saturated NaCl solution, pure water and mineral oil phantoms were made with the same size (a cylindrical bottle with 9-cm long and 5.5-cm diameter). The saturated NaCl phantom with permittivity of about 58 at 400 MHz was used for imaging. The phantoms of pure water and mineral oil were used to test the decoupling performance when some degree of dielectric effects exist at 9.4 T, this dielectric effect may contribute to the coupling between coil elements. In addition, Qs were measured before and after mounting the decoupling inductor to evaluate the loss caused by the additional inductors.

Finally, MRI experiments with this microstrip array was performed on a 9.4 T horizontal bore magnet (Magnex Scientific, UK) interfaced to a Varian INOVA console (Varian Associates, Palo Alto, CA, USA). The gradient-recalled echo (GE) sequences were used (flip angle = 11°, TE = 3.2 ms, TR = 100 ms, matrix size = 128 × 128, field of view = 10 × 10 cm, slice thickness = 3 mm).

2.4. Parallel imaging reconstruction

To demonstrate the parallel imaging performance of the inductively decoupled microstrip array, GRAPPA reconstructions were performed with the phantom data. Partial k-space data were extracted from the full dataset to simulate 2×, 3× and 4× accelerations. The improved GRAPPA reconstruction algorithm reported in Ref. [17] were employed. In each reconstruction, 7 auto-calibrating signal (ACS) lines were used for the fitting process.

3. Results and discussion

The comparison results of the inductive and capacitive decoupling method are shown in Fig. 4. Fig. 4a indicates

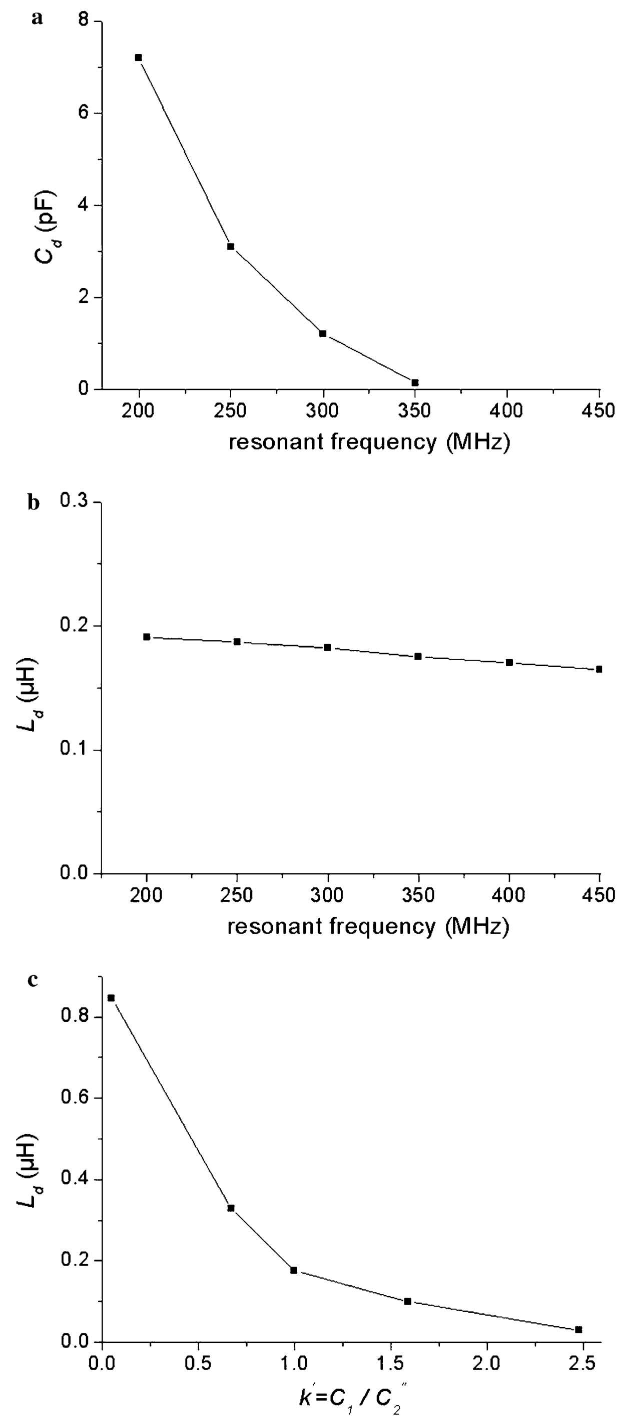

Fig. 4. Experimental comparison between capacitive and inductive decoupling. (a) Interconnecting capacitance and (b) interconnecting inductance, as a function of the resonant frequency. (c) The required decoupling inductor vs. $k' = C'_1/C''_2$ at 400 MHz.

that the decoupling capacitance significantly decreases with the resonant frequency. When the resonant frequency is higher than 350 MHz, the decoupling capacitance is less than 0.3 pF, which is unpractically small. With the same coil geometry, the result of using decoupling inductor is shown in Fig. 4b. Unlike the capacitive decoupling method, the required inductance is almost independent of the resonant frequency. The required inductance is in the range of 0.17–0.19 μH (5–7 turns copper wire with 7 mm diameter). The slight difference of the inductance is caused by the variable k. Because the distributed shunt capacitance of transmission-lines is hard to be estimated, k at different resonant frequencies is not a constant. The comparison indicates that the inductively decoupling method is more appropriate for microstrip arrays at ultrahigh fields. Fig. 4c shows the relationship between $k' = C'_1/C''_2$ and the required decoupling inductance. When k' ranges from 0.05 to 2.5, the required inductance can be controlled in a broad range from 0.03 μH (a 2 cm long copper wire) to 0.84 μH (a 14 turns copper wire with 10 mm diameter) at 400 MHz. Varying the proportion of tuning capacitors, k, is efficient to adjust the decoupling inductances.

The loss of the decoupling circuit is estimated by measuring Q. With one microstrip element resonated at 400 MHz and other seven elements open, the unloaded Q was 130 and the loaded Q was 85 for the saturated NaCl phantom. After mounting decoupling inductors, unloaded Q of all the elements were around 120–130 and loaded Q were around 72–82, no significant loss is observed.

Table 1 illustrates the relation between frequency split and the decoupling inductance. When increasing the decoupling inductor from 0.027 μH to ∞, only one of the split frequencies, f_e, varies with the decoupling inductance and shifted from 403.5 to 391.5 MHz, while f_m almost remains the same. This fact agrees with Eqs. (3) and (4) quite well.

Table 2 shows the decoupling results with different phantoms. Without the decoupling inductors, the mutual coupling between the 1st neighbors split the resonant peaks no matter what phantoms are used. After implementing the decoupling circuit, S_{21} among all the coil elements are better than −13 dB with the saturated NaCl and mineral oil phantoms, and it is about 1–5 dB worse with the pure water phantom. The results demonstrate that even the dielectric effect exists at 9.4 T, this inductive decoupling scheme is still valid.

Although the inductors were connected between the adjacent elements, Table 2 shows that the inductor decoupling method can reduce the mutual coupling not only between adjacent elements, but also between non-adjacent elements. The decoupling inductors bring 3–14 dB additional isolations for all non-adjacent elements, which is shown more clearly in Fig. 5. By connecting the elements to the two ports of a network analyzer, the S_{11}, S_{22} and S_{21} curves of the nearest, 2nd, 3rd, and 4th neighbors are shown in Figs. 5a–d, respectively. S_{21} of the 3rd and 4th neighbors obviously decrease near the 400 MHz. All the L/C components between the non-adjacent elements can be seen as a L/C decoupling network, which is helpful for reducing the mutual coupling. Further study will be needed to analyze and optimize the decoupling scheme for the non-adjacent elements.

Table 1
f_m and f_e of the two adjacent microstrip coils

f_m (MHz)	f_e (MHz)	L_d (μH)
399.1	391.5	∞
399.6	397.0	0.197
400.0	400.0	0.081
400.1	403.5	0.027

With the increase of decoupling inductors, f_e decreases while f_m is unchanged.

Table 2
The required decoupling inductances and S_{21} between coil elements with different phantoms: saturated NaCl, pure water, and mineral oil phantom

Phantom	Neighbors	S_{21} (dB)		L_d (μH)
		Without L_d	With L_d	
Saturated NaCl	1st	Peak splitting	−15 to −20	0.19
	2nd	−10 to −14	−12 to −21	
	3rd	−17 to −21	−24 to −29	
	4th	−19 to −22	−27 to −36	
Pure water	1st	Peak splitting	−13 to −17	0.24
	2nd	−8 to −15	−11 to −21	
	3rd	−14 to −19	−21 to −30	
	4th	−19 to −22	−18 to −26	
Mineral oil	1st	Peak splitting	−14 to −22	0.20
	2nd	−11 to −13	−12 to −19	
	3rd	−18 to −22	−22 to −35	
	4th	−16 to −24	−22 to −25	

L_d was measured at 100 kHz.

Fig. 6a shows the saturated NaCl phantom image acquired from each element. The image profiles indicate that sufficient decoupling among all elements is achieved. Fig. 6b shows a combined image from the individual images by using the sum-of-squares method and 2×, 3×, and 4× accelerated cases using the improved GRAPPA reconstruction algorithm. Those combined images have good quality in terms of SNR and artifacts, implying the inductively decoupled microstrip array is suitable for parallel imaging.

Note that the isolations achieved by this inductively decoupling scheme is very efficient for the receive mode to avoid peak splitting and to attain sufficient decoupling for independent coil tuning and matching. For transmit mode, highly decoupling might be required.

4. Conclusion

This work provides a new and efficient approach for decoupling the microstrip array at ultra-high fields. In contrast to the capacitive decoupling methods, the decoupling inductance is independent of the resonant frequency, making this method much easier to implement. The decoupling inductance can be decreased by varying the tuning capacitors on the strips, such that the self-resonant frequency of

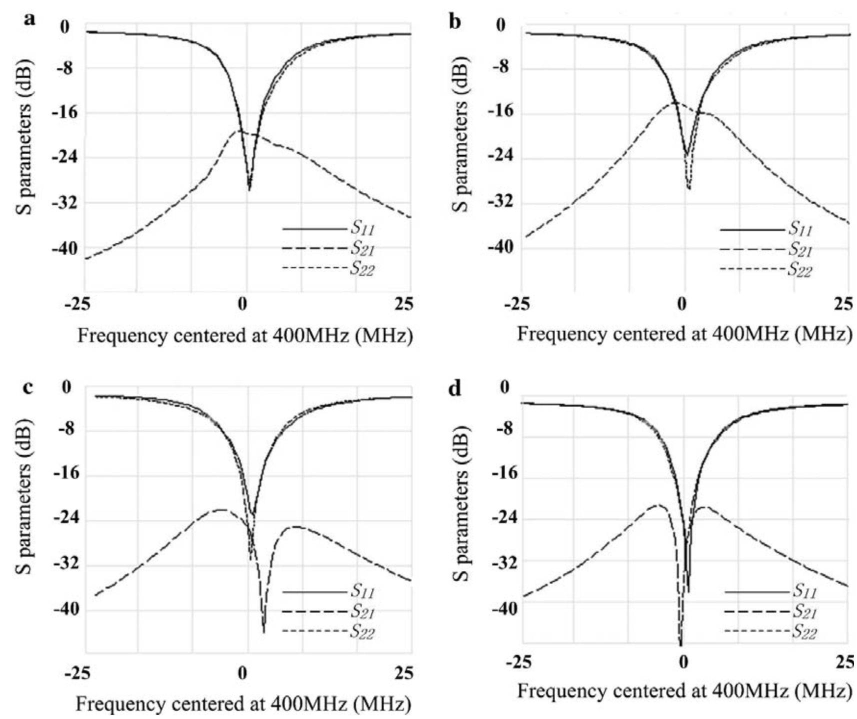

Fig. 5. In the eight-channel microstrip array, the S_{11}, S_{22}, and S_{21} parameters of the nearest neighbor (a), second neighbor (b), third neighbor (c) and forth neighbor (d) after loading with a saturated NaCl phantom. The span is 50 MHz and the central frequency is 400 MHz.

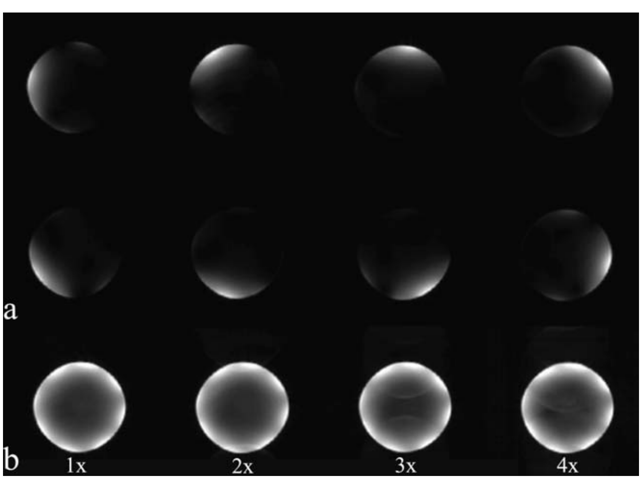

Fig. 6. Images of the saturated NaCl phantom obtained with the eight-channel microstrip array. (a) MR images acquired from each element with a gradient-recalled echo (GE) pulse sequence (TE = 3.2 ms, TR = 100 ms, flip angle = 11°, NEX = 1, FOV = 10 cm, slice thickness = 3 mm, matrix size = 128 ×128). (b) Combined image by using sum-of-square method and images acquired by using improved GRAPPA with 2×, 3×, and 4× acceleration rate.

the decoupling inductors is well beyond the frequency of interest. Size of the inductors, and therefore the loss caused by this decoupling circuit can be also controlled. In our eight-channel prototype at 9.4 T, the interconnecting inductors can reduce the coupling not only between adjacent elements, but also between non-adjacent elements. This decoupling approach has great potential for packing more elements into microstrip arrays for the purpose of parallel imaging and retaining depth sensitivity at fields higher than 7 T.

Acknowledgments

This work was supported by Hong Kong RGC Earmarked Research Grant HKU 7045/01E, 7170/03E, 7168/04E, and NIH Grants R01EB004453, BTRR P41 008079, KECK Foundation, MIND Institute.

References

[1] K.P. Pruessmann, M. Weiger, M.B. Scheidegger, P. Boesiger, SENSE: sensitivity encoding for fast MRI, Magn. Reson. Med. 42 (1999) 952–962.

[2] D.K. Sodickson, W.J. Manning, Simultaneous acquisition of spatial harmonics (SMASH): fast imaging with radiofrequency coil arrays, Magn. Reson. Med. 38 (1997) 591–603.

[3] F. Wiesinger, P.F. Van de Moortele, G. Adriany, N. De Zanche, K. Ugurbil, K.P. Pruessmann, Parallel imaging performance as a function of field strength-an experimental investigation using electrodynamic scaling, Magn. Reson. Med. 52 (2004) 953–964.

[4] P.J. Ledden, J.H. Duyn, Ultra-high frequency array performance: predicted effects of dielectric resonance, in: Proceedings of the ISMRM 10th Annual Meeting, #324, 2002.

[5] G. Adriany, P. Moortele, F. Wiesinger, S. Moeller, J.P. Strupp, P. Andersen, C. Snyder, X. Zhang, W. Chen, K.P. Pruessmann, P. Boesiger, Y. Vaughan, K. Ugurbil, Transmit and receive transmission line arrays for 7 Tesla parallel imaging, Magn. Reson. Med. 53 (2005) 434–445.

[6] G. Adriany G, J. Ritter, P.V. Moortele, S. Moeller, C. Snyder, B. Voje, T. Vaughan, K. Ugurbil, A Geometrically Adjustable 16 Channel Transceive Transmission Line Array for 7 Tesla, in: Proceedings of the ISMRM 13th Annual Meeting, #673, 2005.

[7] C. Snyder, S. Moeller, J. Ritter, P. Moortele, C. Akgun, G. Adriany, K. Ugurbil, T. Vaughan, A Z-Gradient Coil for 3D SENSE Imaging at 7 Tesla, in: Proceedings of the ISMRM 13th Annual Meeting, #674, 2005.
[8] X. Zhang, A.R. Burr, X-H Zhu, G. Adriany, K. Ugurbil, W. Chen, A Dual-tuned Microstrip Volume Coil Array for Human Head Parallel $^{1}H/^{31}P$ MRI/MRS at 7 T, in: Proceedings of the ISMRM 13th Annual Meeting, #896, 2005.
[9] E.B. Boskamp, R.F. Lee, Whole body LPSA transceive array with optimized transmit homogeneity, in: Proceedings of the ISMRM 10th Annual Meeting, #903, 2002.
[10] P.B. Roemer, W.A. Edelstein, C.E. Hayes, S.P. Souza, O.M. Mueller, The NMR phased array, Magn. Reson. Med. 16 (1990) 192–225.
[11] R.F. Lee, R.O. Giaquinto, C.J. Hardy, Coupling and decoupling theory and its application to the MRI phased array, Magn. Reson. Med. 48 (2002) 203–213.
[12] B. Wu, X. Zhang, G.X. Shen, An optimized four-channel microstrip array at 7T, in: Proceedings of the ISMRM 14th Annual Meeting, #2569, 2006.
[13] R.F. Lee, C.J. Hardy, D.K. Sodickson, P.A. Bottomley, Lumped-element planar strip array (LPSA) for parallel MRI, Magn. Reson. Med. 51 (2004) 172–183.
[14] T. Nabeshima, T. Takahashi, Y. Matsunaga, E. Yamamoto, K. Katakura, RF probe for MRI, U.S. patent 5,489,847, 1996.
[15] J.-S. Hong, Microstrip Filters for RF/Microwave Applications, Wiley, New York, 2001.
[16] X. Zhang, K. Ugurbil, W. Chen, Microstrip RF surface coil design for extremely high-field MRI and spectroscopy, Magn. Reson. Med. 46 (2001) 443–450.
[17] P. Qu, G.X. Shen, C. Wang, B. Wu, J. Yuan, Tailored utilization of acquired k-space points for GRAPPA reconstruction, J. Magn. Reson. 174 (2005) 60–67.